THE JOURNAL OF PHYSICAL CHEMISTRY C

Article

Cite This: J. Phys. Chem. C 2019, 123, 7682−7695

pubs.acs.org/JPCC

Proton Transfers at a Dopamine-Functionalized TiO_2 Interface

Costanza Ronchi,[†] Daniele Selli,[†] Waranyu Pipornpong,[†,‡] and Cristiana Di Valentin*[,†]

[†]Dipartimento di Scienza dei Materiali, Università di Milano-Bicocca, via R. Cozzi 55, I-20125 Milano, Italy

[‡]Department of Chemistry, Faculty of Science, Chulalongkorn University, Bangkok 10330, Thailand

Supporting Information

ABSTRACT: Despite the many successful syntheses and applications of dopamine-functionalized TiO_2 nanohybrids, there has not yet been an atomistic understanding of the interaction of this 1,2-dihydroxybenzene derivative ligand with the titanium dioxide surfaces. In this work, on the basis of a wide set of dispersion-corrected hybrid density functional theory (DFT) calculations and density functional tight binding (DFTB) molecular dynamics simulations, we present a detailed study of the adsorption modes, patterns of growth, and configurations of dopamine on the anatase (101) TiO_2 surface, with reference to the archetype of 1,2-dihydroxybenzene ligands, i.e., catechol. At low coverage, the isolated dopamine molecule prefers to bend toward the surface, coordinating the NH_2 group to a Ti_{5c} ion. At high coverage, the packed molecules succeed in bending toward the surface only in some monolayer configurations. When they do, we observe a proton transfer from the surface to the ethyl-amino group, forming terminal NH_3^+ species, which highly interact with the O atoms of a neighboring dopamine molecule. This strong Coulombic interaction largely stabilizes the self-assembled monolayer. On the basis of these results, we predict that improving the probability of dopamine molecules being free to bend toward the surface through thermodynamic versus kinetic growth conditions will lead to a monolayer of fully protonated dopamine molecules.

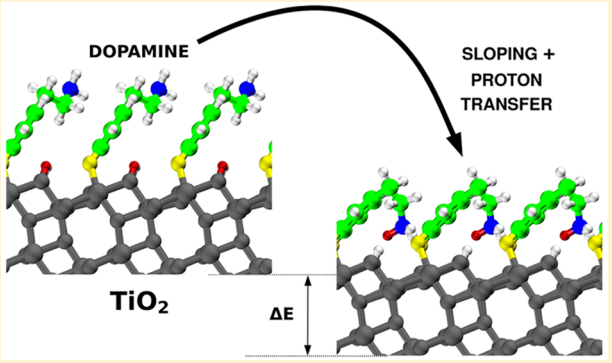

1. INTRODUCTION

Surface modification of titanium dioxide with organic or organometallic molecules has been attracting the attention of the scientific community during the last two decades due to the variety of applications of this material, in particular in photocatalysis and photovoltaic solar cells.[1−3] Under normal conditions, rutile is the most stable bulk TiO_2 polymorph; however, when nanostructured (usually below 20 nm), the anatase phase is preferred[4] with the (101) being the most stable and exposed surface.[5] Furthermore, the anatase allotrope is considered particularly photoactive[6] and, thus, a good candidate to be used in high surface area photocatalytic and photovoltaic devices. A major bottleneck, however, is that anatase TiO_2 only absorbs the ultraviolet light, due to its large band gap of 3.2 eV at room temperature.[7] Surface modification with appropriate organic ligands generally allows tuning the band gap of the bare metal oxide, through a red shift of the adsorption band from the UV to the visible range. Functionalization, for example, with catechol, improves the adsorption of the solar spectrum, refining the performances of the material in photoactivated devices.[8−11] Due to its central role in the electron-transfer process, the adsorption of catechol, which is the archetype for all functionalized 1,2-dihydroxybenzene ligands, on the anatase (101) TiO_2 surface has been widely investigated, both experimentally[12−19] and theoretically, using cluster or surface models.[20−25] Some of the works present in the literature indicate the bidentate adsorption mode as the most stable one.[12,14,19]

More recently, surface modification of TiO_2 has also found application in the modern field of nanomedicine.[26−28] In particular, TiO_2 nanoparticles (NPs) are functionalized in order to build novel bioinorganic hybrid nanoconjugates. In general, these systems are prepared by connecting an inorganic component, such as a metal or metal oxide NP, to biomolecules (e.g., polymers, proteins, DNA fragments). They are used for several biomedical applications, including biocompatibility, multimodal imaging, and targeting of specific cells.[28−31] The use of TiO_2 nanoparticles makes the nanoconjugates perfect candidates for photocatalytic therapy or photoactivated drug release.

However, due to their peculiar surface chemistry, largely determined by the presence of undercoordinated Ti atoms, bare TiO_2 NPs are cytotoxic.[32−34] This problem can be overcome by exploiting the high reactivity exhibited by these undercoordinated sites toward oxygen-rich ligands, as they fill the octahedral coordination sites.[35] Once functionalized, the reactivity of the NPs with cellular proteins is minimized,

Special Issue: Hans-Joachim Freund and Joachim Sauer Festschrift

Received: May 23, 2018
Revised: June 19, 2018
Published: June 20, 2018

DOI: 10.1021/acs.jpcc.8b04921
J. Phys. Chem. C 2019, 123, 7682−7695

reducing potential particle toxicity and eventually assuming site selectivity and functionality.[36]

The additional advantage deriving from functionalization with organic molecules is that they provide the NP with specific binding sites for biomolecules. A successful strategy for attaching biomolecules to the surface of TiO_2 is to exploit a linker with double functional moieties: one anchoring the surface of the metal oxide and the other binding the bioactive molecule. The linkers are organic molecules having oxygen-containing substituents, such as dopac or dopamine.[28,31,35,37−43] Dopamine exhibits a diolic group (two OH) in the catechol-like portion for surface anchoring and one ethyl-amino group ($-CH_2CH_2NH_2$) for the bioactive molecule binding. Moreover, it has been shown to facilitate the charge transfer between the inorganic and biological components.[44]

Dopamine-modified TiO_2 NPs were used to detect and repair DNA mutations or to activate specific oxidation processes, in analogy to endonuclease activity.[28,31] Rajh and co-workers also developed a method to control charge transfer from DNA to TiO_2/dopamine, exploiting the sequence dependent charge separation.[45] Similarly built systems were used to specifically bind proteins, altering cell metabolism and inducing cell death.[42,46,47] Moreover, Thurn et al. synthesized TiO_2/dopamine/DNA nanoconjugates to be used as gene knockout devices and tumor imaging agents at the same time.[48] Dopamine functionalized TiO_2 NPs can also bind proteins or peptides to build up electrochemical biosensors, relevant for drug discovery, diagnostics, environmental applications, as well as food safety.[49,50]

Despite the long list of successful syntheses and applications of dopamine-functionalized TiO_2 nanohybrids, a complete atomistic understanding of the structure, function, and mechanism of these nanodevices is still lacking. Differently from catechol, very little is known about dopamine adsorption on the anatase (101) TiO_2 surface, in particular with regard to the different binding configurations. Most of the works assume that dopamine adsorbs on the TiO_2 surface in a bidentate configuration similar to catechol,[51] while the possible role of the ethyl-amino functionality in the binding to the surface is generally neglected.[52,54] The adsorption of one single molecule of dopamine was studied theoretically by Vega-Arroyo et al. with a TiO_2 cluster model, who stated that the bidissociated bidentate adsorption mode is favored with respect to the monodentate or molecular ones.[52,53] Urdaneta et al. investigated the adsorption of dopamine in a low coverage regime, by considering uniquely a bidentate configuration on different low index anatase surfaces.[54]

From an experimental point of view, the surface of some spherical colloidal NPs was modified with different amounts of dopamine and optically characterized through adsorption and diffuse reflectance spectroscopy;[55] however, the dopamine adsorption mode was not investigated nor discussed. On an anatase TiO_2 (101) single crystal, a photoemission study addressing the adsorption of one monolayer of dopamine molecules suggested the bidentate configuration to be the most likely one, even if no assessment on the actual structure of the monolayer was reported.[44] Therefore, a complete and exhaustive understanding of the mechanism of dopamine adsorption on the anatase TiO_2 (101) surface and of the electronic properties of the resulting hybrid organic/inorganic interface is still lacking.

The aim of this work is to investigate, by means of a wide set of hybrid density functional theory (DFT) calculations including dispersion corrections, the details of the dopamine adsorption on a slab model of the anatase (101) surface of TiO_2 at increasing coverage, up to a full monolayer. The well-known case of catechol is used as a reference for the more complex case of dopamine, comparing various conceivable low coverage adsorption configurations and identifying the modifications caused by the anchoring molecule to the electronic structure of the material. We considered then increasing dopamine coverages in order to establish the molecular layer growth mechanism, under both kinetic and thermodynamic control. To this end, molecular dynamics simulations, based on the self-consistent charge density-functional tight-binding (SCC-DFTB) theory, have also been performed, screening several possible configurations for a full monolayer of dopamine molecules. Some unexpected proton transfers are observed.

The paper is organized as follows: in section 2, we describe the computational details and models used in this work. In section 3, we present our results on the isolated molecule adsorption of catechol and dopamine (section 3.1), on the growth mechanism up to a full monolayer of catechol or dopamine under kinetic control (section 3.2), on the most stable dopamine monolayer structure (section 3.3), and on the possibility of a different thermodynamic growth mechanism (section 3.4). Finally, we present a summary and the relevant conclusions from this study.

2. COMPUTATIONAL DETAILS

For all of the density functional theory (DFT) electronic structure calculations and geometry optimizations, we made use of the CRYSTAL14 simulation package,[56] where the Kohn−Sham orbitals are expanded in Gaussian-type orbitals. The all-electron basis sets are Ti 86-4111 (d41) and O 8-4111 (d1) for TiO_2 and H 5-111 (p1), C 6-31111 (d1), O 8-41111 (d1), and N 6-311 (d1) for the adsorbed catechol and dopamine molecules. We used the HSE06[57] screened hybrid density functional, and we took into account long-range van der Waals interactions with the inclusion of the semiempirical dispersion correction proposed by Grimme (DFT-D2).[58] The cutoff limits in the evaluation of the Coulomb and exchange series/sums were set to 10^{-7} for Coulomb overlap tolerance, 10^{-7} for Coulomb penetration tolerance, 10^{-7} for exchange overlap tolerance, 10^{-7} for exchange pseudo-overlap in the direct space, and 10^{-14} for exchange pseudo-overlap in the reciprocal space. For the geometry optimization, forces were relaxed to be less than 4.5×10^{-4} au and displacements to be less than 1.8×10^{-3} au.

All the self-consistent-charge density functional tight-binding (SCC-DFTB)[59,60] electronic structure calculations, geometry optimizations, and molecular dynamics simulations were performed with the DFTB+ simulation package.[61] We employed the MATORG parametrization set[62] for the pairwise interaction of the atoms of both TiO_2 and adsorbed molecules. The description of the hydrogen bonding has been further improved with the inclusion of the empirical HBD correction ($\zeta = 4$).[63]

Born−Oppenheimer molecular dynamics simulations were performed within the canonical ensemble (NVT). The Newton equations of motion were integrated with the velocity Verlet algorithm, and a relative small time step of 0.5 fs was used to ensure reversibility. A Nosé−Hoover thermostat, with

DOI: 10.1021/acs.jpcc.8b04921
J. Phys. Chem. C 2019, 123, 7682−7695

a time constant of 0.03 ps, kept the temperature at 300 K. After 10 ps of equilibration, the systems were allowed to evolve for another 40 ps. Statistical sampling has been enhanced running four separate simulations for each system, where different random seeds for velocity assignment were considered.

The full optimization of bulk TiO_2 anatase was carried out on the primitive cell using a Monkhorst−Pack *k*-point mesh of 12 × 12 × 12 to ensure the convergence on the electronic part. The values of the optimized lattice parameters for bulk anatase TiO_2 are 3.746 and 3.796 Å for *a* and 9.674 and 9.790 Å for *c* with HSE06-D2 and DFTB(MATORG), respectively. The bandgap (E_g) for bulk anatase (101) has been calculated to be 3.7 eV with HSE06-D2 and 3.3 eV with DFTB(MATORG). In Table 1, these data have been compared with other hybrid DFT functionals[64,65] and experimental values.[66,68]

Table 1. Optimized Cell Parameters *a* and *c* (in Å) and Electronic Band Gap E_g (in eV) of TiO_2 Bulk Anatase Computed with DFT(HSE06) and DFTB(MATORG) and Compared with Other Hybrid DFT Functionals and Experimental Values

method	*a*	*c*	E_g
DFT(HSE06), this work	3.746	9.674	3.7
DFTB(MATORG), this work	3.796	9.790	3.3
DFT(B3LYP)[64]	3.789	9.777	3.8
DFT(PBE0)[65]	3.758	9.704	4.5
Exp.[66]	3.782	9.502	
Exp.[67]			3.4

To model the (101) anatase surface, three triatomic layers of TiO_2 slab were considered. The bottom layer was kept fixed to the optimized bulk positions during the geometry optimization (no periodic boundary conditions were imposed in the direction perpendicular to the surface). To investigate binding energies and equilibrium geometries, we used two supercell models: (i) The 1 × 4 supercell model (144 atoms, see Figure S1 in the Supporting Information) has eight Ti_{5c} (5-fold coordinated) adsorption sites; thus, it allows to model a coverage density of one monolayer, 1 ML (four molecules in the supercell), 0.5 ML (two molecules in the supercell), and 0.25 ML (one molecule in the supercell). (ii) The 2 × 4 supercell model (288 atoms) with 16 Ti_{5c} adsorption sites has been used to model lower coverage densities of 0.125 ML (one molecule in the supercell). Preliminary geometry optimizations were performed at the Γ point, and then, the most stable selected configurations have been further optimized using a *k*-point mesh of 2 × 2 × 1 to ensure the convergence of the electronic structure. The total adsorption energy per molecule has been defined as

$$\Delta E_{ads}^{mol} = (E_{slab+nmol} - [E_{slab} + n_{mol}E_{mol}])/n_{mol}$$

where $E_{slab+nmol}$ is the total energy of the whole system, E_{slab} is the energy of the surface slab, E_{mol} is the energy of the molecule in the gas phase, and n_{mol} is the number of molecules adsorbed on the surface.

The total density of states (DOS) and projected density of states (PDOS) were computed with a finer *k*-point mesh of 30 × 30 × 1. For 3D electron charge density plots of the localized states in the band gap, an isovalue of 0.003 au has been used.

The transition state structure for the protonation of the $-NH_2$ group of a single dopamine molecule to give $-NH_3^+$ on a fully covered 1 × 2 supercell model (72 atoms, 2 dopamine molecules) has been evaluated with the NEB method,[68] as implemented in the Atomic Simulation Environment (ASE).[69] This toolkit is a driver, which we interfaced to the CRYSTAL14 code in order to use its internal NEB algorithm which, otherwise, is not implemented in CRYSTAL14. The NEB procedure was carried out employing seven intermediate images. The reaction barrier for the dissociation process is defined as

$$\Delta E_{diss}^{\ddagger} = E_{TS} - E_{slab+mol}$$

where E_{TS} is the energy of the transition state geometry and $E_{slab+mol}$ is the total energy of the optimized geometry of the dopamine molecules adsorbed on the titania surface with unprotonated $-NH_2$ groups.

3. RESULTS AND DISCUSSION

3.1. Low Coverage: Isolated Molecule Adsorption. In this section, we analyze the adsorption of an isolated molecule of catechol and then of an isolated molecule of dopamine on the anatase (101) TiO_2 surface. First, we define the nomenclature to label the various model structures obtained. Both catechol and dopamine may bind to the five-coordinated titanium (Ti_{5c}) on the anatase surface through one (monodentate, M) or two (bidentate, B) O atoms of the hydroxyl groups, in an undissociated ("U") or dissociated ("D") mode. Upon dissociation, one ("D_1") or two ("D_2") protons are transferred to neighboring surface 2-fold coordinated O atoms (O_{2c}). Finally, dopamine may also bind through the N atom of the amino group in a monodentate fashion ("M^{NH_2}").

We analyzed six different adsorption configurations of catechol, which differ both for the relative position of the molecule with respect to the surface orientation and for the OH dissociation extent. The optimized geometries and the relative HSE06-D2 adsorption energies (ΔE_{ads}^{mol}) are shown in Figure 1. To enucleate the dispersion contribution to ΔE_{ads}^{mol}, we refer to some further data reported in Table S1 in the Supporting Information. The six configurations are (1) monodentate undissociated catechol with the molecular plane parallel to the Ti_{5c} row ($MU_{\parallel}$, Figure 1a); (2) monodentate undissociated catechol with the molecular plane perpendicular to the Ti_{5c} row ($MU_{\perp}$, Figure 1b); (3) monodentate dissociated catechol (MD, Figure 1c); (4) bidentate undissociated catechol (BU, Figure 1d); (5) bidentate singly dissociated catechol (BD_1, Figure 1e); and (6) bidentate doubly dissociated catechol (BD_2, Figure 1f). The angle between the phenyl ring plane and the plane along the Ti_{5c} row (i.e., the [10-1] direction) is 18.76 and 72.29° for $MU_{\parallel}$ and $MU_{\perp}$, respectively. In all of the bidentate structures, the phenyl ring tilts toward the nearest O_{2c} atoms, in agreement with previous studies.[12] For the monodentate geometries, the dispersion interactions between the molecule and the slab play a crucial role. As the distance between the average *z* coordinate of the phenyl ring and the slab decreases, the contribution of the dispersion interactions and, consequently, ΔE_{ads}^{mol} increases. Thus, the order of stability for the monodentate configurations is $MU_{\parallel}$ > MD > $MU_{\perp}$.

As an overall trend, the bidentate geometries of adsorption, already considered by Liu et al.,[12] result in being more stable than the monodentate ones. In the doubly dissociated BD_2, the two dissociated protons are transferred on the nearest and on the farthest neighboring O_{2c} atoms, respectively (see Figure

DOI: 10.1021/acs.jpcc.8b04921
J. Phys. Chem. C 2019, 123, 7682−7695

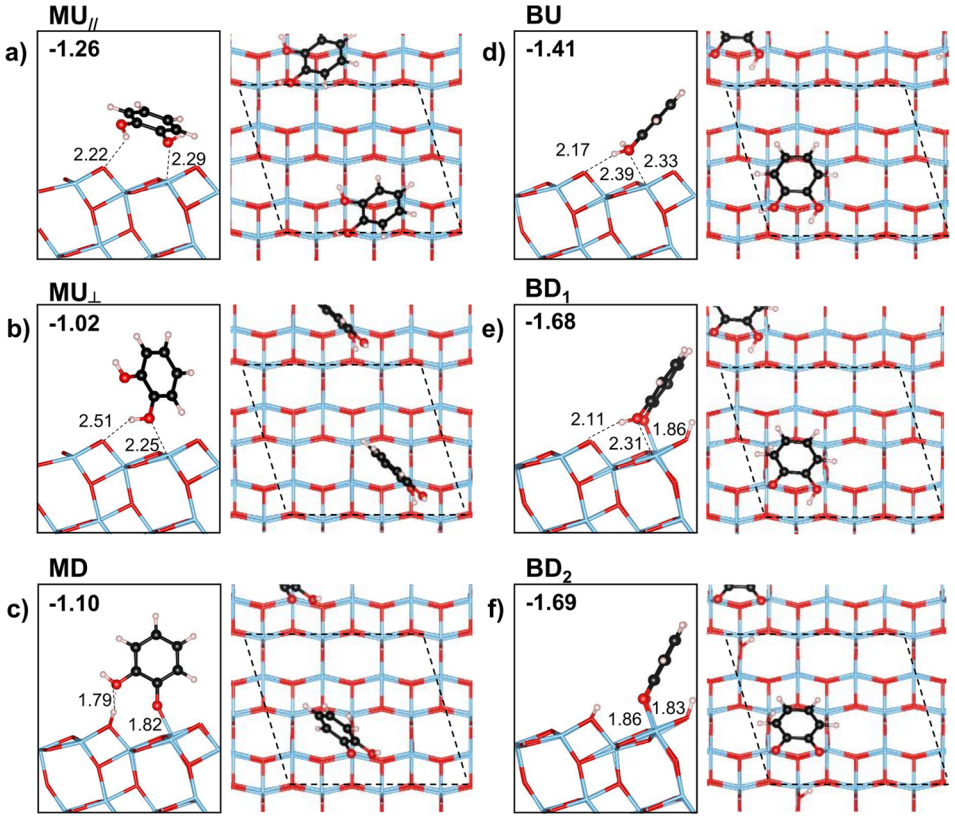

Figure 1. Adsorption modes (side and top views) and adsorption energies per molecule (ΔE_{ads}^{mol}, in eV) for one molecule of catechol on the anatase (101) TiO_2 surface, as obtained by HSE06-D2: (a) monodentate undissociated parallel ($MU_{||}$) to the surface; (b) monodentate undissociated perpendicular ($MU_{\perp}$) to the surface; (c) monodentate dissociated (MD); (d) bidentate undissociated (BU); (e) bidentate singly dissociated (BD_1); (f) bidentate doubly bidissociated (BD_2). The overlying parallelogram in dashed line represents the supercell model used for the calculations. Relevant distances are reported in Å in proximity of the bond stick or dashed line.

1f). For BD_1 and BU, the undissociated hydroxyl groups preferentially form H-bonds with the farthest neighboring O_{2c} atoms of the surface (see Figure 1d and e, respectively). We found that the BD_2 structure is approximately degenerate to BD_1 (−0.01 eV); therefore, in the low coverage regime, both configurations are likely to exist, whereas the molecular adsorbed configuration BU is higher in energy. The contribution of the dispersion energies is nearly constant for the bidentate conformations (around −0.6/0.7 eV for HSE06-D2).

Since we found that the bidentate (singly and doubly) dissociated adsorption modes are the most favored in the case of catechol, those are the ones we will consider for dopamine adsorption. Although dopamine presents many more configurational degrees of freedom than catechol, only few geometries of adsorption have been considered in the literature so far.[50−52] In Figure 2, we report the six most interesting structures among those studied in the present work, with the phenyl ring tilting both toward the nearest surface O_{2c} (three on the left) and toward the nearest O_{3c} atoms (three on the right). The adsorption energies (ΔE_{ads}^{mol}) obtained by HSE06-D2 (and HSE06 on the HSE06-D2 optimized geometry) are summarized in Table S2 in the Supporting Information.

The configurations are (1) bidentate and singly dissociated dopamine with respect to the OH group and monodentate with respect to the NH_2 group binding to a surface Ti_{5c} atom ($B°D_1M^{NH_2}$, Figure 2a); (2) bidentate and doubly dissociated dopamine with respect to the OH groups ($B°D_2$ in Figure 2b); and (3) bidentate and doubly dissociated with respect to the OH groups and monodentate with respect to the NH_2 group binding a surface Ti_{5c} atom ($B°D_2M^{NH_2}$, Figure 2c). We always started the relaxation from the bidentate configuration, but in one case, this evolved into a monodentate species ($M°D_1M^{NH_2}$, see Figure 2a). In the $B°D_2$ adsorption mode, the amino-ethyl group ($-CH_2CH_2NH_2$) stands up toward the vacuum, while, in $B°D_2M^{NH_2}$, the molecule bends toward the surface to allow the binding of the $-NH_2$ group to a Ti_{5c} and the formation of H-bonds with the surface O_{2c}. $B°D_2$ is the dopamine corresponding structure for the BD_2 with catechol (Figure 1f), and it is the only bidentate configuration that was previously reported in the literature for dopamine. However, we find that it is the least stable among those considered in this work, by about 1 eV (see Table S2 in the Supporting Information). Furthermore, since for $B°D_2$ there is no additional interaction of the $-CH_2CH_2NH_2$ group with the surface, the molecule can be indifferently tilted toward the O_{2c} or toward the O_{3c} (the two structures are perfectly isoenergetic, ΔE_{ads}^{mol} = −1.64 eV). On the other hand, both for $B°D_1M^{NH_2}$ and $B°D_2M^{NH_2}$, the configurations bent toward the O_{3c} are slightly more favored, due to a larger interaction of the ring with the underlying surface. Since $B°D_2M^{NH_2}$ is the most stable adsorption mode (ΔE_{ads}^{mol} = −2.91 eV) and the relative stability with respect to $B°D_1M^{NH_2}$ is −0.24 eV, such a structure is expected to be the predominant one in the low coverage regime. This conclusion is different from what was found for catechol, where BD_2 and BD_1 structures are likely to coexist, as discussed above.

DOI: 10.1021/acs.jpcc.8b04921
J. Phys. Chem. C 2019, 123, 7682−7695

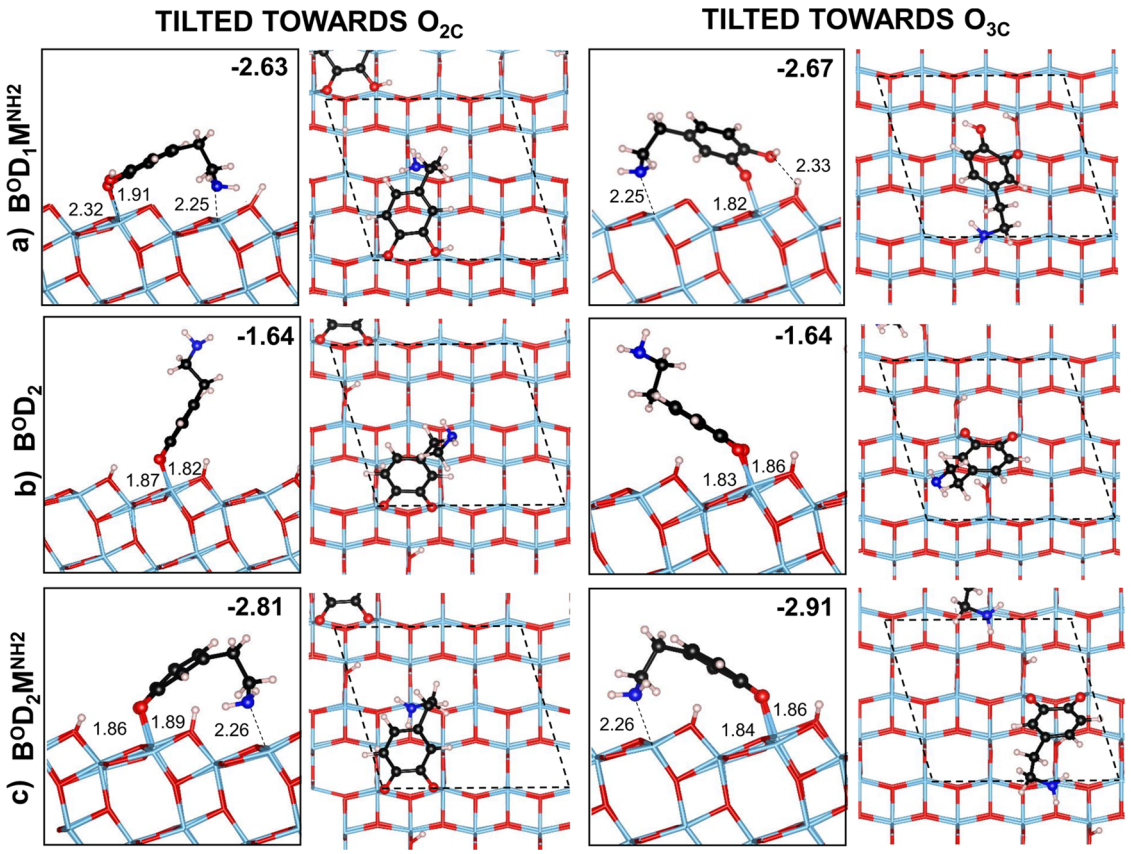

Figure 2. Adsorption modes (side and top views) and adsorption energies per molecule (ΔE_{ads}^{mol}, in eV) for one molecule of dopamine on the anatase (101) TiO_2 surface, as obtained by HSE06-D2. The molecules can be tilted both toward the O_{2c} atoms of the surface (left panel) and toward the O_{3c} (right panel). (a) Singly dissociated bidentate with respect to OH and monodentate with respect to NH_2 ($B^{\circ}D_1M^{NH_2}$) when tilted toward O_{2c} and singly dissociated monodentate ($M^{\circ}D_1M^{NH_2}$) when tilted toward O_{3c}; (b) bidentate doubly dissociated with respect to OH ($B^{\circ}D_2$); (c) bidentate doubly dissociated with respect to OH and monodentate with respect to NH_2 ($B^{\circ}D_2M^{NH_2}$). The overlying parallelogram in dashed line represents the supercell model used for the calculations. Relevant distances are reported in Å in proximity of the bond stick or dashed line.

For the most stable $B^{\circ}D_2M^{NH_2}$ adsorption configuration of dopamine, both OH groups are dissociated and, consequently, two protons are transferred to surface O_{2c} atoms. We considered different H positions, as detailed in Figure S1 and in Table S2 in the Supporting Information, to define which is the lowest energy one, i.e., one H on the O_{2c} just under the phenyl ring and the other H on a O_{2c} in the next parallel row (see Figure 2c).

Finally, we also evaluated the cell size effect on the absorption energy values by means of a larger surface model (2 × 4 supercell, with 16 Ti_{5c} sites). Only $B^{\circ}D_1M^{NH_2}$ resulted in being slightly stabilized, with ΔE_{ads}^{mol} = −2.71 eV (vs −2.67 eV in the 1 × 4 supercell). This result further confirms that, at low coverage, this is the principal adsorption mode for dopamine molecules on the anatase (101) TiO_2 surface.

3.1.1. Electronic Properties. In this section, we investigate and compare the electronic structure of the most stable configurations identified in the previous section both for catechol and for dopamine. In Table 2, we report the values for the electronic band (E_g) and HOMO−LUMO ($\Delta_{HOMO-LUMO}$) gaps calculated for the anatase TiO_2(101) slab, the BD_2 (even if it is nearly isoenergetic with BD_1 at low coverage, it was found to be predominant at increasing coverage),[12] and $B^{\circ}D_2M^{NH_2}$ structures for catechol and dopamine, respectively. The $\Delta_{HOMO-LUMO}$ gap is defined as the difference between the highest occupied state introduced by the adsorbed molecule and the bottom of the conduction band (CB). As it can be seen, the band gap (E_g) is essentially not affected by the adsorption of one single molecule of catechol BD_2 or dopamine $B^{\circ}D_2M^{NH_2}$ (E_g = 4.11 eV for the slab alone and E_g = 4.12 eV with the molecules adsorbed). The $\Delta_{HOMO-LUMO}$ gap is evaluated to be 2.15 eV for BD_2 catechol and 2.26 eV for dopamine $B^{\circ}D_2M^{NH_2}$, which indicates a sensible red-shift of the optical band gap of the TiO_2 surface resulting from the adsorption. In addition, for both systems, we have calculated the total (DOS) and projected density of states (PDOS) in the range between −5 and +5 eV, with reference to the Fermi energy of the system. The electronic structures (Figure 3) for catechol BD_2 and dopamine $B^{\circ}D_2M^{NH_2}$ are shown in parts a and b of Figure 3, respectively, and present several analogies. The 3D charge density plots for the midgap states arising in the presence of the adsorbed single molecule of catechol and

Table 2. Electronic (E_g) and HOMO−LUMO ($\Delta_{HOMO-LUMO}$) Band Gap in eV for One Single Molecule of Catechol BD_2 and Dopamine $B^{\circ}D_2M^{NH_2}$ Adsorbed on the Anatase (101) TiO_2 Surface, as Calculated by HSE06-D2

	E_g (eV)	$\Delta_{HOMO-LUMO}$ (eV)
bare TiO_2 surface	4.11	
TiO_2 + catechol (BD_2)	4.12	2.15
TiO_2 + dopamine ($B^{\circ}D_2M^{NH_2}$)	4.12	2.26

DOI: 10.1021/acs.jpcc.8b04921
J. Phys. Chem. C 2019, 123, 7682−7695

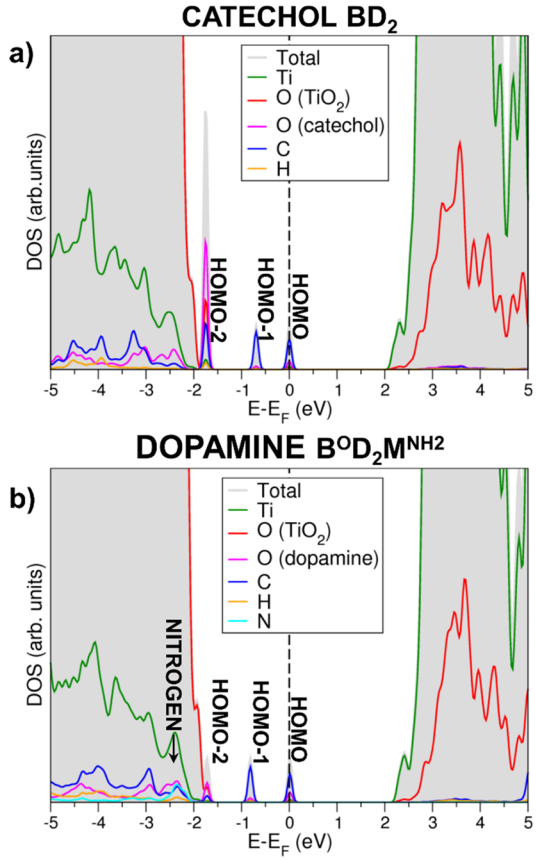

Figure 3. Total (DOS) and projected (PDOS) density of states for low coverage adsorption of a single molecule of (a) catechol BD_2 and (b) dopamine $B^{\circ}D_2M^{NH_2}$ on the anatase (101) TiO_2 surface. The zero energy reference is set at the Fermi energy of the system and highlighted by a dotted line.

dopamine are reported in Figure S2 and Figure S3 in the Supporting Information, respectively.

The peak placed at lowest energy (HOMO−2) is mainly due to the p state of the O atoms of the molecule, while the other two states (HOMO−1 and HOMO) are related to the π and π^* orbitals of the C atoms of the phenyl ring. It is possible to see that, differently from HOMO and HOMO−1 states, which are totally localized on the molecule, the electronic density for HOMO−2 has a contribution also from the nearest surface O_{3c} atoms. For dopamine $B^{\circ}D_2M^{NH_2}$, the peak relative to the p states of N is placed inside the valence band and the 3D charge density plot is reported in Figure S4 in the Supporting Information. This is due to the formation of a bond between N and the underneath Ti_{5c}, increasing the hybridization of the molecule with the surface.

3.2. Growth Mechanism. In this section, we focus on the growth mechanism of one full monolayer of catechol and then of dopamine molecules on the TiO_2 anatase (101) surface. We assume that deposition takes place under kinetic control and, therefore, molecules quickly arrange on the surface one after the other, before the ethyl-amino functionality of dopamine has time to bend toward the surface. We will give more insights about the possible final and thermodynamically more stable configurations and adsorption patterns of the full monolayer of dopamine molecules in the next section (3.3). The molecules are considered to grow in the bidentate adsorption mode: BD_2 for catechol (see image on left side, central row of Figure 4), which was found to be the most stable adsorption mode at increasing coverage,[12] and up_NH_2 for dopamine (see image on left side, bottom row of Figure 4).

The up_NH_2 adsorption mode is a doubly dissociated bidentate configuration only slightly different with respect to $B^{\circ}D_2$ (see section 3.1, Figure 2b) due to the different orientation of the amino-ethyl functionality. In the up_NH_2 adsorption mode, this points upward, toward the vacuum, and does not interact with the surface (see Figure 4), as suggested by previous studies.[51−53] This is not the only possible adsorption mode for dopamine (neither the most stable, see section 3.3), but it is the one we expect to observe in the initial phase of the self-assembling growth process.

In the bidentate modes above, molecules bind two of the eight Ti_{5c} sites present in the 1 × 4 supercell; therefore, at full coverage, four molecules adsorb. The adsorption energies at increasing coverage for catechol BD_2 are reported in Table 3, whereas the adsorption configurations for 0.5 and 1.0 ML coverage regimes are shown in Figure S5 in the Supporting Information and Figure 4 (middle row), respectively. To enucleate the dispersion contribution to ΔE_{ads}^{mol}, we refer to some further data reported in Table S3 in the Supporting Information.

At 0.5 ML coverage, the second catechol molecule can bind either next to the first, thus on the same Ti_{5c} row ("0.5 ML[same row]" in Table 3 and Figure S1a in the Supporting Information), or on the parallel Ti_{5c} row ("0.5 ML[diff. row]" in Table 3 and Figure S1b in the Supporting Information), along the [11-1] direction and zigzag ("0.5 ML[zig-zag]" in Table 3 and Figure S1c in the Supporting Information). The last two configurations are nearly isoenergetic and are favored by −0.34/−0.35 eV with respect to the first one.

For the full coverage regime of bidentate molecules, three different patterns are possible, as represented in Figure 4: the already mentioned growth along the [11-1] direction (Figure 4a), the symmetrically equivalent one along the [1-1-1] direction (Figure 4b), and the zigzag growth (Figure 4c), modeled by means of an orthorhombic cell. According to our calculation, the zigzag pattern is isoenergetic with those along the [11-1] and [1-1-1] directions in the case of catechol. Experimentally, however, Liu et al. observed by means of an STM (scanning tunneling microscope) study that an adsorbed monolayer of catechol molecules on the anatase (101) TiO_2 surface forms elongated islands along the two symmetric directions [11-1] and [1-1-1].[12] Therefore, for some kinetic reasons that do not emerge from our static calculations, the zigzag pattern is not experimentally observed.

In the case of a just deposited dopamine monolayer (up_NH_2 configuration), we obtain again similar energies for the corresponding three possible growth directions ([11-1], [1-1-1], and zigzag, as shown in the bottom row of Figure 4). Since in this case no experimental STM image is reported in the literature, we cannot exclude the possibility of a zigzag type growth pattern, as discussed in the next section (3.3).

3.3. Full Coverage of Dopamine. In this section, we discuss in detail the different possible minimum structures for a full monolayer of dopamine molecules. We will first focus on the [11-1] growth direction (see Figure 4a). More configurations for the monolayer of the up_NH_2 dopamine molecules are possible than the ones shown in Figure 4a, depending on the relative orientation of the $-CH_2CH_2NH_2$ group with respect to the [010] direction. The equilibrium structures, the schemes of adsorption patterns, and the relative

DOI: 10.1021/acs.jpcc.8b04921
J. Phys. Chem. C 2019, 123, 7682−7695

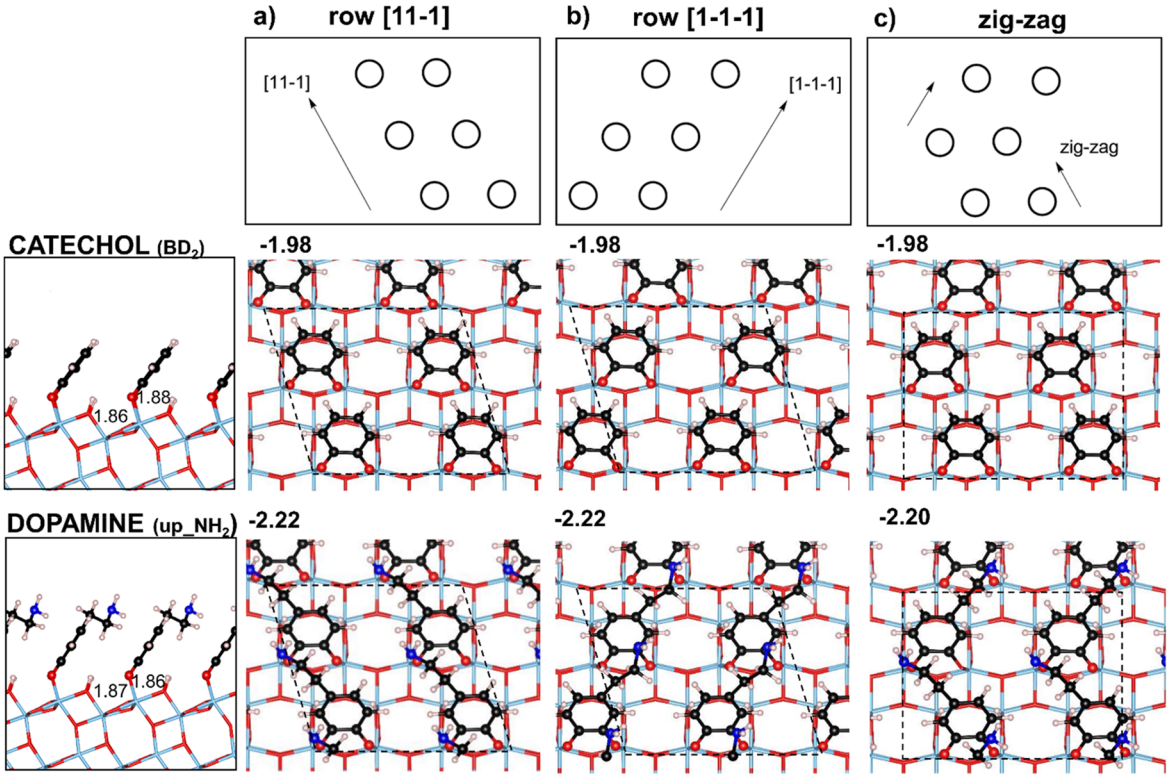

Figure 4. Adsorption modes (side and top view) for different growing patterns and adsorption energies per molecule (ΔE_{ads}^{mol}, in eV) for a full monolayer (1.0 ML) of bidentate BD_2 catechol (upper panel) or bidentate up_NH_2 dopamine molecules (lower panel) on the anatase (101) TiO_2 surface, as calculated by HSE06-D2. The growth of the full monolayer is schematically represented at the top: (a) along the [11-1] row; (b) along the [1-1-1] row; and (c) with a zigzag pattern. The overlying parallelogram or rectangle in dashed line represents the supercell model used for the calculations. Relevant distances are reported in Å in proximity of the bond stick.

Table 3. Adsorption Energies per Molecule (ΔE_{ads}^{mol}, in eV) for Different Growing Patterns and Coverages of Catechol BD_2 Adsorbed on the Anatase (101) TiO_2 Surface, as Calculated by HSE06-D2[a]

BD_2 catechol coverage	N. Occ Ti_{5c}	N. molecules	ΔE_{ads}^{mol} (eV), HSE06-D2
0.25 ML	2/8	1	−1.69
0.5 ML [same row]	4/8	2	−1.62
0.5 ML [diff. row]	4/8	2	−1.96
0.5 ML [zigzag]	4/8	2	−1.97
1.0 ML [11-1] or [1-1-1]	8/8	4	−1.98
1.0 ML [zigzag]	8/8	4	−1.99

[a]For the labeling, refer to Figure 1, Figure S5 in the Supporting Information, and Figure 4.

adsorption energies are reported in Figure 5. More specifically, the $-CH_2CH_2NH_2$ functional group of the four dopamine molecules can be all LEFT-oriented (up_NH_2(LL), Figure 5a), mixed RIGHT/LEFT (up_NH_2(RL), Figure 5b) or LEFT/RIGHT (up_NH_2(LR), Figure 5c), or all RIGHT-oriented (up_NH_2(RR), Figure 5d). These adsorption patterns are nearly isoenergetic, and their appearance is consequently equally probable from a thermodynamic point of view. This fact has crucial consequences on the final adsorption structure of the dopamine molecules composing the monolayer on anatase (101) TiO_2, as we will extensively discuss in the following.

In order to investigate how the temperature will affect the rearrangement of the as-deposited up_NH_2 dopamine molecules in the three possible configurations, we performed three DFTB molecular dynamics runs at 1 atm and 300 K. To monitor the dynamical behavior of different configurations considered, we plotted the $p(z)$ distributions of the vertical (z) component of the distance between the N atom of the dopamine molecules and the Ti_{5c} atoms of the surface (see Figure 6). In the case of up_NH_2(RR) (black line in Figure 6), all of the functional groups which initially are oriented toward the vacuum rotate during the simulation, allowing the N atoms of each dopamine molecule to bend down toward the slab (as shown going from Figure 7a to Figure 7b). This gives rise to a major peak of the $p(z)$ at ∼3.5 Å, thus having the N atom very close to the surface. In the case of up_NH_2(RL) (blue line in Figure 6), only for half of the dopamine molecules (the ones with the ethyl-amino functionalities RIGHT-oriented) it is possible to rotate their functional groups and to bend toward the surface because of the steric hindrance of another dopamine molecule in front of them. Thus, the $p(z)$ presents two peaks: one at ∼3.5 Å, relative to the molecules that bent down, and one at ∼6.5 Å relative to the molecules (LEFT-oriented) that cannot bend down. For the up_NH_2(LL) configuration (red line in Figure 6), all of the N atoms remain at ∼6.5 Å, since none of functional groups have the space to bend down toward the surface. In this last case, we can notice the presence of a second small peak at around 4.5−5 Å in the $p(z)$ distribution. This is due to a partial rotation of the $-CH_2CH_2NH_2$ group induced by the temperature, which does not result in the complete sloping toward the surface.

The result of the MD simulation starting from an up_NH_2(RR) configuration is schematically represented in the first part of Figure 7a and b. As a result of a rotation, we

DOI: 10.1021/acs.jpcc.8b04921
J. Phys. Chem. C 2019, 123, 7682−7695

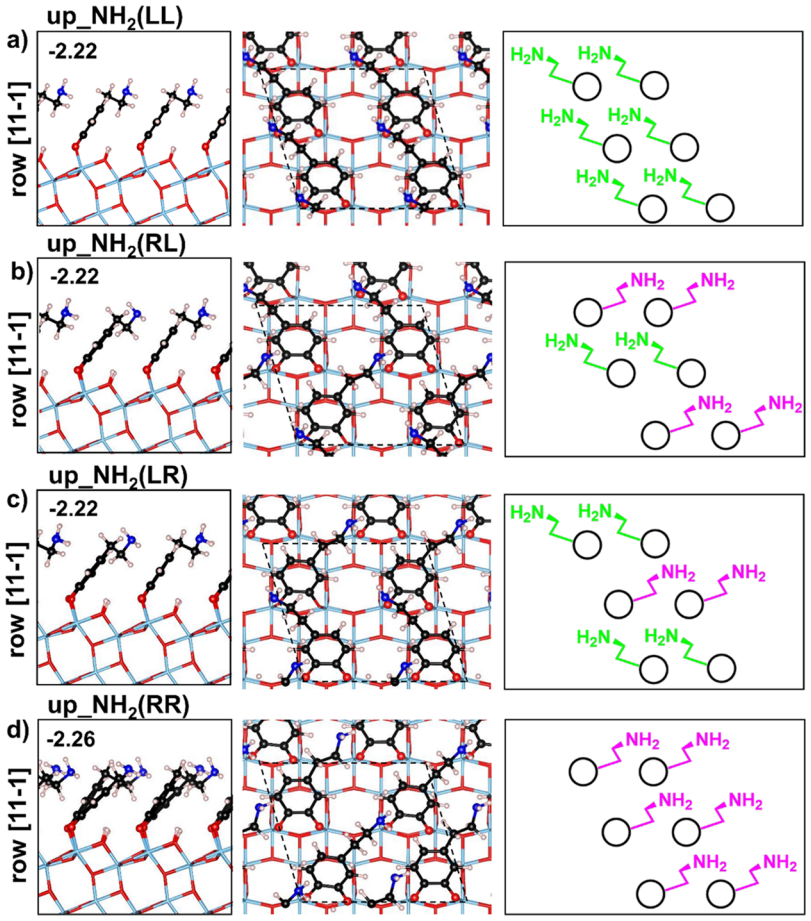

Figure 5. Adsorption modes (side and top view), adsorption energies per molecule (ΔE_{ads}^{mol}, in eV), and schematic top view sketch of the $-CH_2CH_2NH_2$ functionality for a full monolayer of dopamine molecules: (a) up_NH_2(LL), (b) up_NH_2(RL), (c) up_NH_2(LR), and (d) up_NH_2(RR) adsorbed on the anatase (101) TiO_2 surface. LEFT-oriented and RIGHT-oriented functional groups are marked in green and purple, respectively. The overlying parallelogram in dashed line represents the supercell model used for the calculations.

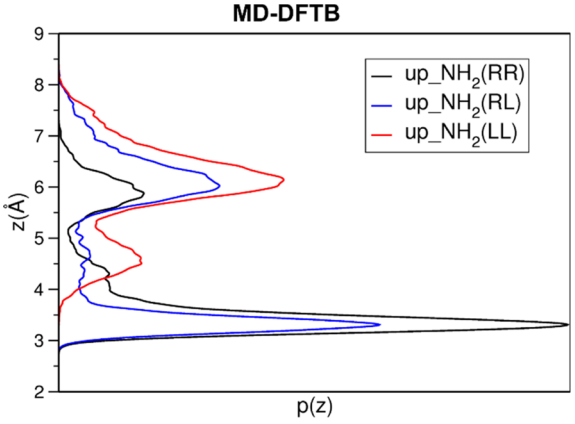

Figure 6. DFTB distribution $p(z)$ of the vertical z component of the distances between the N atoms of the ethyl-amino group of the dopamine monolayer and the (101) anatase TiO_2 surface (Ti_{5c} atoms). Colors refer to the different initial configurations, up_NH_2(RR) in black, up_NH_2(RL) in blue, and up_NH_2(LL) in red.

observe a bidentate down_NH_2(RR) structure (Figure 7b), where all of the amino-ethyl groups have sloped down and H-bonding with the anchoring O atoms of two neighboring dopamine molecules on the next parallel Ti_{5c} row (see the scheme in Figure 7). This down_NH_2(RR) structure is extremely stable (ΔE_{ads}^{mol} = −2.63 eV), almost −0.40 eV more stable than up_NH_2(RR) (see Table 4). We can estimate the barrier for the process of $-CH_2CH_2NH_2$ rotation/bending to be of the order of kT (25 meV), where k is the Boltzmann constant, since this process occurred within the first 10 ps of the MD at 300 K.

When the dopamine molecules bind the surface through a bidentate adsorption mode, the protons deriving from the dissociation of the OH groups saturate all of the O_{2c} of the surface forming bridging $O_{2c}H$ groups. Therefore, since at the full coverage there is such a high density of bridging $O_{2c}H$ groups formed on the surface, we considered the possibility that some of the protons are transferred to the NH_2 moieties of the dopamine molecules, resulting in the formation of R−NH_3^+ groups. Indeed, we found that this is a thermodynamically favorable process for all four molecules, leading to the formation of a very stable structure (ΔE_{ads}^{mol} = −3.12 eV), the down_NH_3^+(RR) structure (Figure 7c). Each proton transfer is associated with an energy stabilization of nearly −0.15 eV (see Table S4 in the Supporting Information). All adsorption energies are detailed in Table 4. Some other less stable optimized structures examined throughout this work are reported in Figure S6, and all of the ΔE_{ads}^{mol} are listed in Table S4 in the Supporting Information.

To confirm that the protonation of the R−NH_2 groups of the dopamine molecules to form R−NH_3^+ is feasible from a

DOI: 10.1021/acs.jpcc.8b04921
J. Phys. Chem. C 2019, 123, 7682−7695

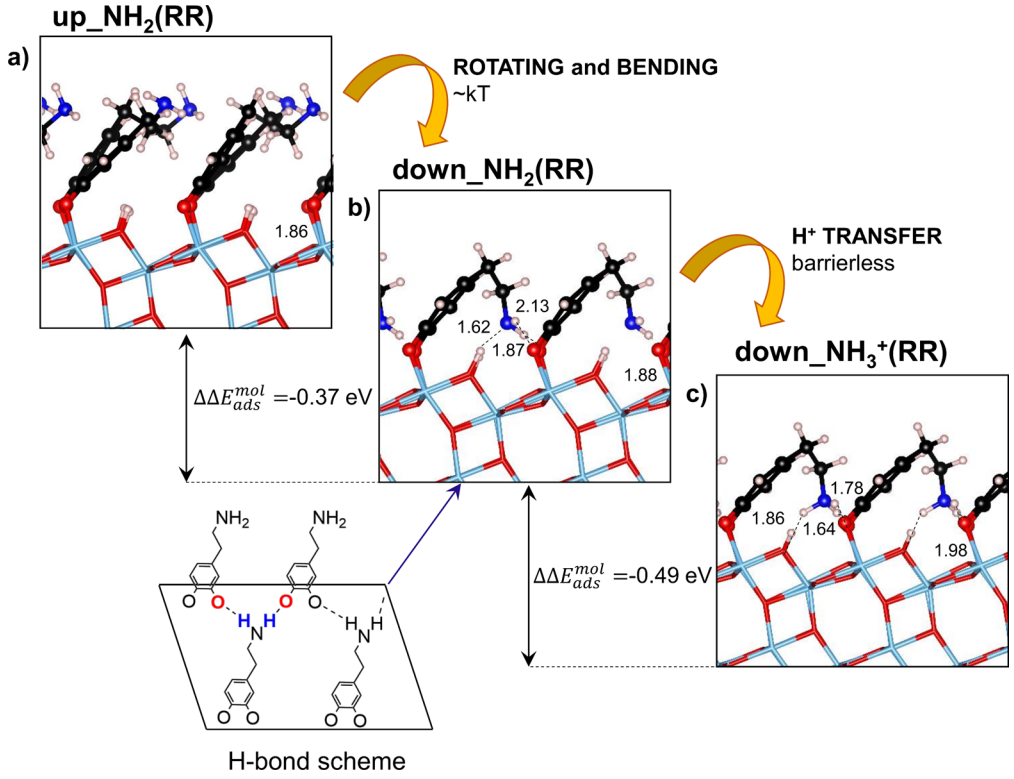

Figure 7. Process of rotation and protonation of the adsorbed dopamine molecules in the full coverage regime, starting from (a) the up_NH_2(RR) configuration, resulting in (b) the down_NH_2(RR) structure and followed by the protonation, which yields (c) the down_NH_3^+(RR) structure. Adsorption energy per molecule (ΔE_{ads}^{mol}, in eV) and differences of adsorption energy between configurations ($\Delta\Delta E_{ads}^{mol}$) are reported. On the left bottom corner, we show a scheme of H-bonding for the full monolayer of dopamine molecules in the down_NH_2(RR) configuration. Relevant distances are reported in Å in proximity of the bond stick or dashed line.

Table 4. Adsorption Energy per Molecule (ΔE_{ads}^{mol}, in eV) for the Possible Configurations Reached during the Formation of a Full Monolayer of Dopamine, as Calculated by HSE06-D2[a]

ΔE_{ads}^{mol} HSE06-D2	row [11-1] tilted toward O_{2c}	zigzag
up_NH_2(RR)	−2.26	
up_NH_2(RL)	−2.22	−2.20
up_NH_2(LR)	−2.22	
up_NH_2(LL)	−2.22	
down_NH_2(RR)	−2.63	
down_NH_3^+(RR)	−3.12	−3.06

[a]For the labeling, refer to Figure 4, Figure 5, and Figure 7.

kinetic point of view, we computed the activation barrier by means of nudged elastic band calculations (NEB). The process is found to be barrierless, so we can conclude that, when and if the R−NH_2 group of a dopamine molecule gets close to the anatase (101) TiO_2 surface, there will be a spontaneous proton transfer from the surface O_{2c}H to the R−NH_2 group.

Differently from the low coverage regime, where all of the configurations considered are most stable if the phenyl ring is tilted toward the O_{3c} atom of the surface (see Figure 2 in section 3.1 and Table S2 in the Supporting Information), at full coverage, a larger stability is observed when the phenyl ring is tilted toward the O_{2c}. For the most favorable down_NH_3^+, the difference is of −0.27 eV in favor of the tilting toward the O_{2c}.

On the basis of the results obtained so far, (i) all of the up_NH_2 configurations in Figure 5 are almost isoenergetic (see also Table 4), (ii) the −$CH_2CH_2NH_2$ tend to rotate and slope down (as observed during the DFTB-MD simulations), (iii) the proton transfer from O_{2c}H to the R−NH_2 is barrierless, and (iv) down_NH_3^+ is the thermodynamically most favorable adsorption mode, we may infer what are the possible scenarios for the different patterns of a full monolayer of dopamine molecules along the [11-1] row on the anatase (101) TiO_2 surface. The configuration where all of the molecules are RIGHT-oriented (up_NH_2(RR) in Figure 5d) results in a structure where 100% of −$CH_2CH_2NH_2$ groups slope down and consequently accept a proton from the surface, leading to the formation of down_NH_3^+(RR) (see Figure 8a). On the other hand, the configuration where all of the molecules are LEFT-oriented (up_NH_2(LL)) along the [11-1] direction (see Figure 5a) remains 100% up, with the nonprotonated NH_2 group, since there is not sufficient space for the −$CH_2CH_2NH_2$ groups to rotate and bend down toward the surface. Finally, the mixed 50% RIGHT/LEFT (up_NH_2(RL) in Figure 5b) or LEFT/RIGHT (up_NH_2(LR) in Figure 5c) configurations will result in 50% up_NH_2 and 50% down_NH_3^+ structure (see Figure S6e in the Supporting Information). Therefore, overall, the proportion between the dopamine molecules up_NH_2 and the protonated molecules down_NH_3^+ present on the surface is 50:50. Our conclusions provide a solid rationalization of the experimental observations by Syres et al., based on photoemission spectra (XPS) of one monolayer of dopamine molecules on the anatase TiO_2(101) surface.[43] The measurements detected the presence of NH_2 and of another N-containing species, whose binding energy is

DOI: 10.1021/acs.jpcc.8b04921
J. Phys. Chem. C 2019, 123, 7682−7695

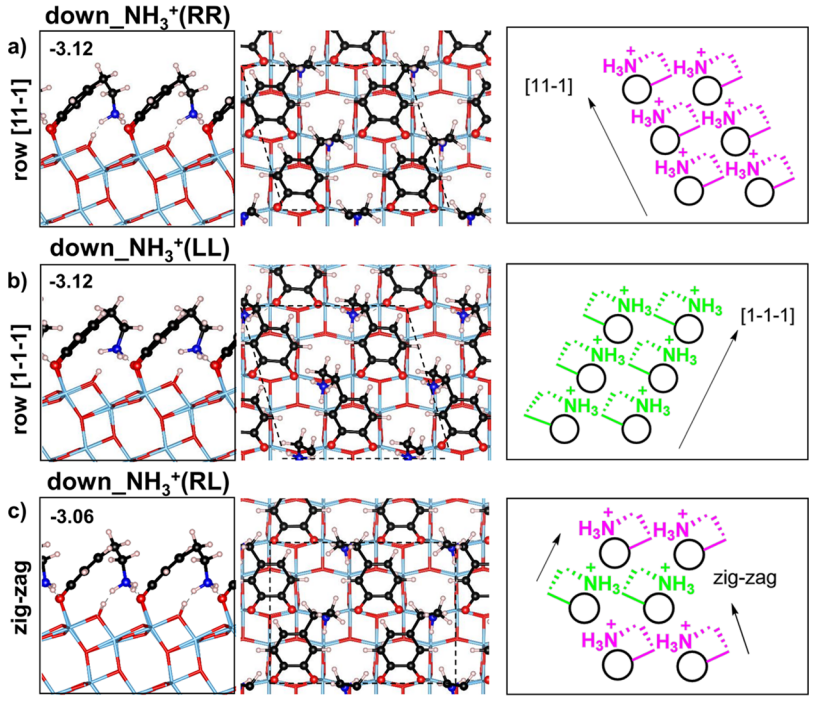

Figure 8. Possible growing patterns and related adsorption energies per molecule (ΔE_{ads}^{mol}, in eV) for a full monolayer of down_NH_3^+ dopamine molecules on the anatase (101) TiO_2 surface, as calculated by HSE06-D2. Growth of the full monolayer is reported (a) along the [11-1] row, (b) along the [1-1-1] row, and (c) with a zigzag pattern. The overlying parallelogram or rectangle in dashed line represents the supercell model used for the calculations.

consistent with that of the NH_3^+ group, with a proportion of nearly 50:50.

This scenario holds not only for the case of the dopamine molecules deposited along the [11-1] direction but also for the cases along the [1-1-1] direction and with the zigzag pattern (see section 3.2 for definitions). For all three of these cases, there is a proper orientation of the ethyl-amino groups, which allows the rotation, the sloping, and the consequent protonation, forming the thermodynamic most stable down_NH_3^+structures (see Figure 8), but also an improper orientation, which prevents such motion of the ethyl-amino groups, leaving all of the dopamine molecules in the up_NH_2 configuration, and finally a mixed configuration, where up_NH_2 and down_NH_3^+ are equally represented.

In particular, regarding the case of the growth along the [1-1-1] row, it results to be symmetrically equivalent to the [11-1]: when the molecules on the surface assemble with the functional group RIGHT-oriented (Figure 4b), they assume an up_NH_2 adsorption configuration, since there is not enough space for the $-CH_2CH_2NH_2$ rotation. On the contrary, when they are LEFT-oriented, the dopamine molecules will arrange to reach the most stable down_NH_3^+ structure (Figure 8b). The case in which the molecules are half RIGHT- and half LEFT-oriented results in a mixed 50% up_NH_2 and 50% down_NH_3^+ structure for full coverage.

Even in a zigzag growth regime, there are configurations, with alternating LEFT- and RIGHT-oriented groups, where the molecules are prevented from sloping down, such as the one in Figure 4c, and configurations, with alternating RIGHT- and LEFT-oriented groups, where the molecules find enough space to slope down, producing the down_NH_3^+ pattern (see Figure 8c). If the functional groups are all RIGHT- or all LEFT-oriented, 50% of the molecules are expected to be up_NH_2 and 50% to be down_NH_3^+.

Overall, independently from the deposition pattern considered, in a full monolayer of dopamine molecules on the anatase (101) TiO_2 surface, we expect to observe an average of 50% of dopamine molecules standing up and preserving the NH_2 group and 50% of protonated molecules (NH_3^+), as a result of the rotation and sloping of the ethyl-amino functionality.

3.3.1. Electronic Properties. In this section, we investigate and compare the electronic structure of one full monolayer of dopamine molecules in the up_NH_2(RR) and down_NH_3^+(RR) configurations adsorbed on anatase (101) TiO_2 in terms of the total (DOS) and projected density of states (PDOS) in the range between −5 and +5 eV with reference to the Fermi energy of the system. The electronic structures for the up_NH_2(RR) and down_NH_3^+(RR) configurations are shown in Figure 9. We report in Table 5 the values for the electronic (E_g) and HOMO−LUMO ($\Delta_{HOMO-LUMO}$) band gap for the two structures.

The PDOS of up_NH_2(RR) (Figure 9a) presents five midgap states. The HOMO is predominantly constituted by one π state of the phenyl ring with a major contribution from the C atoms, whereas the HOMO−1 is localized on two equivalent N atoms of the dopamine molecule. Also, the HOMO−2 state is mainly constituted by the p states of the nitrogen atoms, while the HOMO−3 has a strong contribution of the bonding π orbital of the carbon atoms of the phenyl ring. The HOMO−4 is formed by the p states of the anchoring oxygen states of the dopamine molecules, hybridized with those from the O atoms of the TiO_2 surface.

The PDOS of the down_NH_3^+(RR) full monolayer structure (Figure 9b) presents only three midgap states. The HOMO and HOMO−1 are essentially π orbitals of the C atoms of the phenyl ring. The HOMO−2 state has a major contribution from the O atom states of the adsorbed dopamine molecules. Differently from up_NH_2(RR), there are no

DOI: 10.1021/acs.jpcc.8b04921
J. Phys. Chem. C 2019, 123, 7682−7695

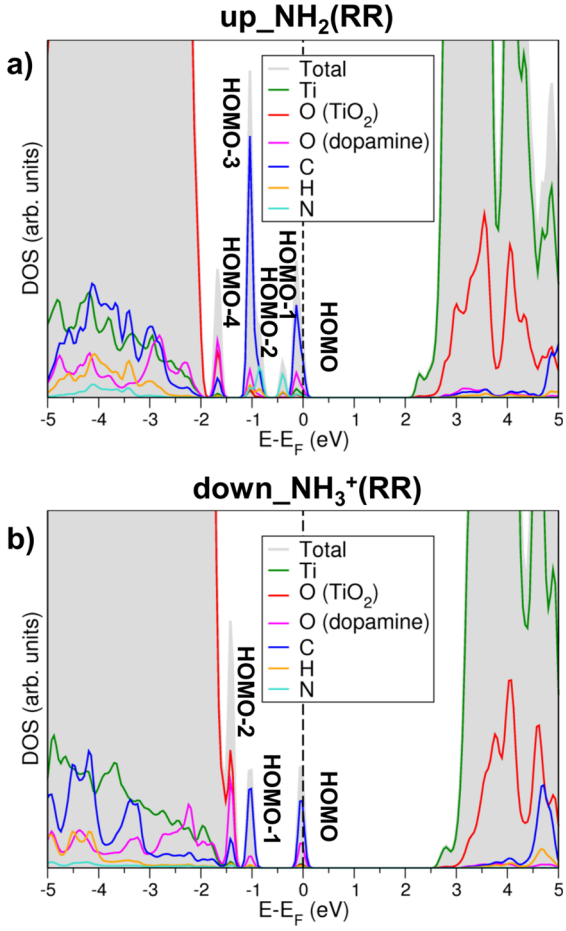

Figure 9. Total (DOS) and projected (PDOS) density of states for the adsorption of one full monolayer of dopamine molecules: (a) up_NH_2(RR) and (b) down_NH_3^+(RR) on the anatase (101) TiO_2 surface. The zero energy reference is set at the Fermi energy of the system and highlighted by a dotted line.

Table 5. Electronic (E_g) and HOMO−LUMO ($\Delta_{HOMO-LUMO}$) Band Gaps in eV for One Full Monolayer of Dopamine Molecules Adsorbed on the Anatase (101) TiO_2 Surface in the up_NH_2(RR) and down_NH_3^+ Configurations, as Calculated by HSE06-D2

	E_g (eV)	$\Delta_{HOMO-LUMO}$ (eV)
up_allNH_2	4.16	2.20
down_NH_3^+	4.32	2.66

midgap states related to the N atom, which are deep inside the valence band, because of the large stabilization effect due to the positive charge. For the same reason, both the electronic (E_g = 4.33 eV) and the optical ($\Delta_{HOMO-LUMO}$ = 2.66 eV) band gaps are wider for down_NH_3^+ with respect to the up_NH_2(RR) configuration (see Table 5). The 3D charge density plots for the midgap states arising in the presence of the adsorbed dopamine molecules are reported in Figure S7 and Figure S8 in the Supporting Information, respectively.

3.4. Thermodynamic Growth. As discussed at the beginning of section 3.2, the patterns investigated so far are those expected under kinetic control. The paramount assumption is that the self-assembling process, namely, the mechanism of adsorption of one dopamine molecule after the other on the surface of TiO_2, takes place before any added molecule has the time to bend down toward the surface. In this last section, we wish to discuss what would happen under thermodynamic control. Under these conditions, we expect that 100% of dopamine molecules will bend down and receive a proton from the surface, leading to the down_NH_3^+ adsorption mode, as we will describe in the following.

Under thermodynamic control, the self-assembling process to a full monolayer of dopamine molecules on anatase (101) occurs so slowly that there is sufficient time for the ethyl-amino group of the first adsorbed dopamine molecule to bend down toward the surface and/or eventually move to another adsorption site before a second molecule reaches the surface. Indeed, the dopamine molecules may have certain mobility on the surface, through the flipping from one Ti_{5c} atom of the surface to another by rotation around one Ti−O bond. The thermodynamic growth is, therefore, completely different from the kinetic growth presented in section 3.2.

We can consider the growth along the [11-1] row as a case study (see Figure 10) and analyze an initial situation where the

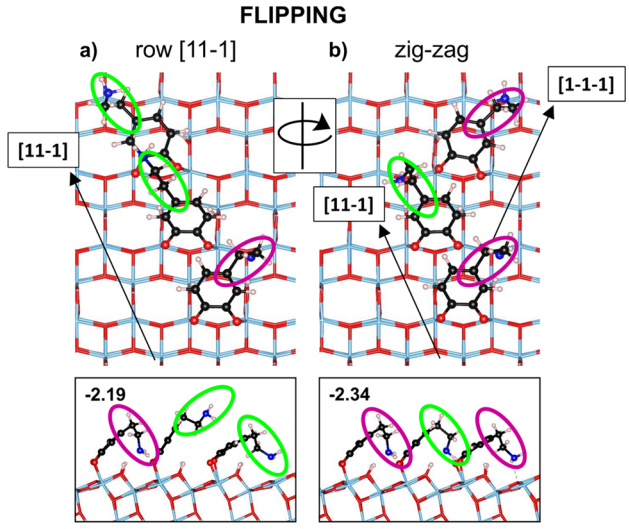

Figure 10. Scheme showing top and side (from the [10-1] direction) views for two different growing mechanisms: (a) growth along the [11-1] row and (b) with a zigzag pattern (after the flipping of the third dopamine molecule) and their relative adsorption energies per molecule (ΔE_{ads}^{mol}, in eV). LEFT-oriented and RIGHT-oriented functional groups are marked in green and purple, respectively.

first molecule is adsorbed with the ethyl-amino group as RIGHT-oriented. A second molecule will adsorb on the closest available position along the [11-1] direction, with the first dopamine molecule bending toward the surface. We considered the case where the ethyl-amino functionality of the second molecule is LEFT-oriented (note that RIGHT orientation was already considered in down_NH_2(RR) in section 3.3). Then, a third dopamine molecule binds the surface. If it anchors along the [11-1] row, there is not enough space for the bending of the second LEFT-oriented molecule. Therefore, the second molecule remains up_NH_2 (see side view in the bottom of Figure 10a), unless the third dopamine molecule flips, rotating around the Ti−O bond (Figure 10b). After flipping, the third molecule would occupy a bonding position along the [1-1-1] row, allowing the second LEFT-oriented molecule to slope down (see side view in the bottom of Figure 10b). The adsorption energy per molecule for the zigzag pattern (Figure 10b) is −2.34 eV, which is −0.15 eV

DOI: 10.1021/acs.jpcc.8b04921
J. Phys. Chem. C 2019, 123, 7682−7695

more favored than the one along the [11-1] row (−2.19 eV). This means that, if the bending and the flipping are in the same time scale of the self-assembling (thermodynamic growth), the totality of the dopamine molecules will arrange in a way that their ethyl-amino functionality is allowed to bend toward the surface and accept a proton, resulting in 100% down_NH_3^+ configuration at the full coverage.

4. CONCLUSIONS

In summary, in this work, we have first investigated, analyzed, and compared the adsorption configurations and electronic structure of catechol and dopamine when adsorbed on the anatase (101) TiO_2 surface at low coverage. Isolated catechol molecules preferentially bind in two bidentate modes (BD_1 and BD_2 in Figure 1), where either one or two protons are transferred to the surface. These two structures are essentially isoenergetic. Dopamine presents a larger number of degrees of freedom, given the added $-CH_2CH_2NH_2$ functional group. The most stable structure is bidentate ($B°D_2M^{NH_2}$ in Figure 2), tilting toward the O_{3c} side, coordinating the NH_2 group with a surface Ti_{5c} and with the two dissociated protons on different Ti_{5c} rows. The electronic structure analysis (Figure 3) for these stable adsorption structures of catechol and dopamine indicates similar features: three gap states are present, with those deriving from dopamine being slightly deeper.

Second, we investigated the growth mechanism of molecular monolayers under kinetic control, i.e., under fast molecular deposition time. Under these conditions, molecules are expected to quickly arrange on the surface one after the other. In the case of dopamine, the consequence is that self-assembling takes place before the ethyl-amino group bends toward the surface (up_NH_2 models). We identified three isoenergetic growth paths: along the [11-1] and [1-1-1] rows and zigzag (Figure 4). Note that in the case of catechol experimental STM images show only the first two.[12]

In the case of dopamine, we have further investigated all of the possible configurations for the growth path along the [11-1] direction. The ethyl-amino group introduces the possibility of various configurations, as shown in Figure 5, for the up_NH_2 structures (RR, RL, LR, and LL). Again, energy differences are negligible. However, starting from these structures and providing some temperature in a molecular dynamics simulation (with DFTB), we observe that the $-CH_2CH_2NH_2$ bends down (down_NH_2), whenever possible, and receives a proton from the oxide surface, forming a $-CH_2CH_2NH_3^+$ species (down_NH_3^+); see Figure 7. Kinetic barriers for these processes are found to be very low or null. However, not all configurations allow the ethyl-amino bending and the proton transfer due to steric hindrance. Therefore, we expect that 50% of the molecules will be bent and protonated, whereas 50% of them will be standing upward and not deprotonated. Analogous results are predicted for the [1-1-1] direction of growth and for the zigzag. Our analysis and conclusions provide a solid rationalization for the experimental observations by Syres et al. based on photoemission spectra of one monolayer of dopamine molecules on the anatase (101) TiO_2 surface.[43] The proton transfer from the surface to the dopamine moiety observed at full coverage affects the electronic structure of the hybrid organic/inorganic system. At full coverage down_NH_3^+, the dopamine states are rather stabilized by the positive charge from the proton (Figure 3b vs Figure 9b).

Finally, we have considered what would differ if the growth took place under thermodynamic control. Under these conditions, molecules have time to diffuse, flip, or bend on the surface; therefore, they all would be able to reach their thermodynamic minimum at full coverage, being all protonated and bent toward the surface (see Figure 10 and related discussion).

To conclude, this study, based on a wide set of hybrid density functional theory calculations including dispersion forces, provides a clear scenario for the adsorption modes, patterns of growth, and configurations of dopamine on the anatase (101) TiO_2 surface, with reference to the archetype of 1,2-dihydroxybenzene ligands, i.e., catechol. We concluded that, at low coverage, the isolated dopamine molecule prefers to bend toward the surface, coordinating the NH_2 group to a Ti_{5c} ion. At high coverage, the packed molecules succeed in bending toward the surface only in some monolayer configurations. When they do, a proton is transferred from the surface to the ethyl-amino group, forming terminal NH_3^+ species, which highly interact with the O atoms of a neighboring dopamine molecule. This strong Coulombic interaction largely stabilizes the self-assembled layer. On the basis of these results, we predict that improving the probability of dopamine molecules being free to bend toward the surface through thermodynamic versus kinetic growth conditions will lead to a monolayer of fully protonated dopamine molecules.

■ ASSOCIATED CONTENT

Supporting Information

The Supporting Information is available free of charge on the ACS Publications website at DOI: 10.1021/acs.jpcc.8b04921.

Tables reporting adsorption energies for one single molecule of catechol or dopamine on TiO_2; table reporting adsorption energies for different growing patterns and coverage of catechol; table reporting adsorption energies for a full monolayer of dopamine molecules; labeling for the possible position of dissociated H atoms on the TiO_2 surface; 3D charge density plots of the midgap states for one single molecule of catechol and of dopamine; 3D charge density plots of the nitrogen midgap state for one single molecule of dopamine; adsorption configurations for half coverage of catechol; adsorption configurations for full coverage of dopamine; 3D charge density plots of the midgap states for full coverage of catechol and of dopamine (PDF)

■ AUTHOR INFORMATION

Corresponding Author

*E-mail: cristiana.divalentin@unimib.it.

ORCID

Cristiana Di Valentin: 0000-0003-4163-8062

Notes

The authors declare no competing financial interest.

■ ACKNOWLEDGMENTS

The authors are grateful to Andrew Thomas at The University of Manchester for fruitful discussions and to Lorenzo Ferraro for his technical help. The project has received funding from the European Research Council (ERC) under the European

DOI: 10.1021/acs.jpcc.8b04921
J. Phys. Chem. C 2019, 123, 7682−7695

Union's HORIZON2020 research and innovation programme (ERC Grant Agreement No. [647020]).

REFERENCES

(1) Grätzel, M. Photoelectrochemical Cells. *Nature* **2001**, *414*, 338−344.
(2) Diebold, U. The Surface Science of Titanium Dioxide. *Surf. Sci. Rep.* **2003**, *48*, 53−229.
(3) Henderson, M. A. A. Surface Science Perspective on TiO_2 Photocatalysis. *Surf. Sci. Rep.* **2011**, *66*, 185−297.
(4) Zhang, H.; Banfield, J. F. Thermodynamic Analysis of Phase Stability of Nanocrystalline Titania. *J. Mater. Chem.* **1998**, *8*, 2073−2076.
(5) De Angelis, F.; Di Valentin, C.; Fantacci, S.; Vittadini, A.; Selloni, A. Theoretical Studies on Anatase and Less Common TiO_2 Phases: Bulk, Surfaces, and Nanomaterials. *Chem. Rev.* **2014**, *114*, 9708−9753.
(6) Kavan, L.; Grätzel, M.; Gilbert, S. E.; Klemenz, C.; Scheel, H. J. Electrochemical and Photoelectrochemical Investigation of Single-Crystal Anatase. *J. Am. Chem. Soc.* **1996**, *118*, 6716−6723.
(7) Hanaor, D. A. H.; Sorrell, C. C. Review of the Anatase to Rutile Phase Transformation. *J. Mater. Sci.* **2011**, *46*, 855−874.
(8) Neouze, M.; Schubert, U. Surface Modification and Functionalization of Metal and Metal Oxide nanoparticles by Organic Ligands. *Monatsh. Chem.* **2008**, *139*, 183−195.
(9) Faure, B.; Salazar-Alvarez, G.; Ahniyaz, A.; Villaluenga, I.; Berriozabal, G.; De Miguel, Y. R.; Bergström, L. Dispersion and Surface Functionalization of Oxide Nanoparticles for Transparent Photocatalytic and UV-Protecting Coatings and Sunscreens. *Sci. Technol. Adv. Mater.* **2013**, *14*, 023001.
(10) Abuabara, S. G.; Rego, L. G. C.; Batista, V. S. Influence of Thermal Fluctuations on Interfacial Electron Transfer in Functionalized TiO_2 Semiconductors. *J. Am. Chem. Soc.* **2005**, *127*, 18234−18242.
(11) Rajh, T.; Nedeljkovic, J. M.; Chen, L. X.; Poluektov, O.; Thurnauer, M. C. Improving Optical and Charge Separation Properties of Nanocrystalline TiO_2 by Surface Modification with Vitamin C. *J. Phys. Chem. B* **1999**, *103*, 3515−3519.
(12) Liu, L. M.; Li, S. C.; Cheng, H.; Diebold, U.; Selloni, A. Growth and Organization of an Organic Molecular Monolayer on TiO_2: Catechol on Anatase (101). *J. Am. Chem. Soc.* **2011**, *133*, 7816−7823.
(13) Nawrocka, A.; Zdyb, A.; Krawczyk, S. Stark Spectroscopy of Charge-Transfer Transitions in Catechol-Sensitized TiO_2 Nanoparticles. *Chem. Phys. Lett.* **2009**, *475*, 272−276.
(14) Syres, K. L.; Thomas, A. G.; Flavell, W. R.; Spencer, B. F.; Bondino, F.; Malvestuto, M.; Preobrajenski, A.; Grätzel, M. Adsorbate-Induced Modification of Surface Electronic Structure: Pyrocatechol Adsorption on the Anatase TiO_2 (101) and Rutile TiO_2 (110). *J. Phys. Chem. C* **2012**, *116*, 23515−23525.
(15) Li, S.-C.; Losovyj, Y.; Diebold, U. Adsorption-Site-Dependent Electronic Structure of Catechol on the Anatase TiO_2 (101). *Langmuir* **2011**, *27*, 8600−8604.
(16) Creutz, C.; Chou, M. H. Binding of Catechols to Mononuclear Titanium(IV) and to 1- and 5-nm TiO_2 Nanoparticles. *Inorg. Chem.* **2008**, *47*, 3509−3514.
(17) Finkelstein-Shapiro, D.; Davidowski, S. K.; Lee, P. B.; Guo, C.; Holland, G. P.; Rajh, T.; Gray, K. A.; Yarger, J. L.; Calatayud, M. Direct Evidence of Chelated Geometry of Catechol on TiO2 by a Combined Solid-State NMR and DFT Study. *J. Phys. Chem. C* **2016**, *120*, 23625−23630.
(18) Lana-Villarreal, T.; Rodes, A.; Pérez, J. M.; Gomez, R. A Spectroscopic and Electrochemical Approach to the Study of the Interactions and Photoinduced Electron Transfer between Catechol and Anatase Nanoparticles in Aqueous Solution. *J. Am. Chem. Soc.* **2005**, *127*, 12601−12611.
(19) Moser, J.; Punchihewa, S.; Infelta, P. P.; Grätzel, M. Surface Complexation of Colloidal Semiconductors Strongly Enhances Interfacial Electron-Transfer Rates. *Langmuir* **1991**, *7*, 3012−3018.
(20) Sánchez-de-Armas, R.; San-Miguel, M.; Oviedo, J.; Márquez, A.; Sanz, J. F. Electronic Structure and Optical Spectra of Catechol on TiO_2 Nanoparticles from Real Time TD-DFT Simulations. *Phys. Chem. Chem. Phys.* **2011**, *13*, 1506−1514.
(21) Rego, L. G. C.; Batista, V. S. Quantum Dynamics Simulations of Interfacial Electron Transfer in Sensitized TiO_2 Semiconductors. *J. Am. Chem. Soc.* **2003**, *125*, 7989−7997.
(22) Lin, H.; Fratesi, G.; Selçuk, S.; Brivio, G. P.; Selloni, A. Effects of Thermal Fluctuations on the Structure, Level Alignment, and Absorption Spectrum of Dye-Sensitized TiO_2: A Comparative Study of Catechol and Isonicotinic Acid on the Anatase (101) and Rutile (110) Surfaces. *J. Phys. Chem. C* **2016**, *120*, 3899−3905.
(23) Xu, Y.; Chen, W.-K.; Liu, S. H.; Cao, M. J.; Li, J. Q. Interaction of Photoactive Catechol with TiO_2 Anatase (101) Surface: A Periodic Density Functional Theory Study. *Chem. Phys.* **2007**, *331*, 275−282.
(24) Redfern, P. C.; Zapol, P.; Curtiss, L. A.; Rajh, T.; Thurnauer, M. C. Computational Studies of Catechol and Water Interactions with Titanium Oxide Nanoparticles. *J. Phys. Chem. B* **2003**, *107*, 11419−11427.
(25) Di Valentin, C.; Fittipaldi, D. Hole Scavenging by Organic Adsorbates on the TiO2 Surface: A DFT Model Study. J. *J. Phys. Chem. Lett.* **2013**, *4*, 1901−1906.
(26) Rajh, T.; Dimitrijevic, N. M.; Bissonnette, M.; Koritarov, T.; Konda, V. Titanium Dioxide in the Service of the Biomedical Revolution. *Chem. Rev.* **2014**, *114*, 10177−10216.
(27) Ghosh, S.; Das, A. P. Modified Titanium Oxide (TiO_2) Nanocomposites and Its Array of Applications: A Review. *Toxicol. Environ. Chem.* **2015**, *97*, 491−514.
(28) Paunesku, T.; Rajh, T.; Wiederrecht, G.; Maser, J.; Vogt, S.; Stojićević, N.; Protić, M.; Lai, B.; Oryhon, J.; Thurnauer, M.; Woloschak, G. Biology of TiO_2−Oligonucleotide Nanocomposites. *Nat. Mater.* **2003**, *2*, 343−346.
(29) Mano, S. S.; Kanehira, K.; Sonezaki, S.; Taniguchi, A. Effect of Polyethylene Glycol Modification of TiO_2 Nanoparticles on Cytotoxicity and Gene Expressions in Human Cell Lines. *Int. J. Mol. Sci.* **2012**, *13*, 3703−3717.
(30) Lopez, T.; Ortiz, E.; Alvarez, M.; Navarrete, J.; Odriozola, J. A.; Martinez-Ortega, F.; Paez-Mozo, E. A.; Escobar, P.; Espinoza, K. A.; Rivero, I. A. Study of the Stabilization of Zinc Phthalocyanine in Sol-Gel TiO_2 for Photodynamic Therapy Applications. *Nanomedicine* **2010**, *6*, 777−785.
(31) Rajh, T.; Saponjic, Z.; Liu, J.; Dimitrijevic, N. M.; Scherer, N. F.; Vega-Arroyo, M.; Zapol, P.; Curtiss, L. A.; Thurnauer, M. C. Charge Transfer Across the Nanocrystalline-DNA Interface: Probing DNA Recognition. *Nano Lett.* **2004**, *4*, 1017−1023.
(32) Trouiller, B.; Reliene, R.; Westbrook, A.; Solaimani, P.; Schiestl, R. H. Titanium Dioxide Nanoparticles Induce DNA Damage and Genetic Instability in Vivo in Mice. *Cancer Res.* **2009**, *69*, 8784−8789.
(33) Oberdorster, G.; Ferin, J.; Gelein, R.; Soderholm, S. C.; Finkelstein, J. Role of the Alveolar Macrophage in Lung Injury: Studies with Ultrafine Particles. *Environ. Health Perspect.* **1992**, *97*, 193−199.
(34) Hamzeh, M.; Sunahara, G. I. In Vitro Cytotoxicity and Genotoxicity Studies of Titanium Dioxide (TiO2) Nanoparticles in Chinese Hamster Lung Fibroblast Cells. *Toxicol. In Vitro* **2013**, *27*, 864−873.
(35) Rajh, T.; Chen, L. X.; Lukas, K.; Liu, T.; Thurnauer, M. C.; Tiede, D. M. Surface Restructuring of Nanoparticles: An Efficient Route for Ligand-Metal Oxide Crosstalk. *J. Phys. Chem. B* **2002**, *106*, 10543−10552.
(36) Ray, P. C.; Yu, H.; Fu, P. P. Toxicity and Environmental Risks of Nanomaterials: Challenges and Future Needs. *J. Environ. Sci. Health C Environ. Carcinog Ecotoxicol Rev.* **2009**, *27*, 1−35.
(37) Weng, Y.-X.; Li, L.; Liu, Y.; Wang, L.; Yang, G.-Z. Surface-Binding Forms of Carboxylic Groups on Nanoparticulate TiO_2 Surface Studied by the Interface-Sensitive Transient Triplet-State Molecular Probe. *J. Phys. Chem. B* **2003**, *107*, 4356−4363.

DOI: 10.1021/acs.jpcc.8b04921
J. Phys. Chem. C 2019, 123, 7682−7695

(38) Vittadini, A.; Selloni, A.; Rotzinger, F. P.; Grätzel, M. Formic Acid Adsorption on Dry and Hydrated TiO2 Anatase (101) Surfaces by DFT Calculations. *J. Phys. Chem. B* **2000**, *104*, 1300−1306.
(39) de la Garza, L.; Saponjic, Z. V.; Dimitrijevic, N. M.; Thurnauer, M. C.; Rajh, T. Surface States of Titanium Dioxide Nanoparticles Modified with Enediol Ligands. *J. Phys. Chem. B* **2006**, *110*, 680−686.
(40) Di Valentin, C.; Costa, D. Anatase TiO_2 Surface Functionalization by Alkylphosphonic Acid: A DFT+D Study. *J. Phys. Chem. C* **2012**, *116*, 2819−2828.
(41) Luschtinetz, R.; Frenzel, J.; Milek, T.; Seifert, G. Adsorption of Phosphonic Acid at the TiO_2 Anatase (101) and Rutile (110). *J. Phys. Chem. C* **2009**, *113*, 5730−5740.
(42) Rozhkova, E. A.; Ulasov, I.; Lai, B.; Dimitrijevic, N. M.; Lesniak, M. S.; Rajh, T. A High-Performance Nanobio Photocatalyst for Targeted Brain Cancer Therapy. *Nano Lett.* **2009**, *9*, 3337−3342.
(43) Duan, D.; Liu, H.; Xu, Y.; Han, Y.; Xu, M.; Zhang, Z.; Liu, Z. Activating TiO_2 Nanoparticles: Gallium-68 Serves as a High-Yield Photon Emitter for Cerenkov-Induced Photodynamic Therapy. *ACS Appl. Mater. Interfaces* **2018**, *10*, 5278−5286.
(44) Syres, K. L.; Thomas, A. G.; Bondino, F.; Malvestuto, M.; Gratzel, M. Dopamine Adsorption on Anatase TiO_2(101): A Photoemission and NEXAFS Spectroscopy Study. *Langmuir* **2010**, *26*, 14548−14555.
(45) Liu, J.; de la Garza, L.; Zhang, L.; Dimitrijevic, N. M.; Zuo, X.; Tiede, D. M.; Rajh, T. Photocatalytic Probing of DNA Sequence by Using TiO_2/Dopamine-DNA Triads. *Chem. Phys.* **2007**, *339*, 154−163.
(46) Dimitrijevic, N. M.; Rozhkova, E.; Rajh, T. Dynamics of Localized Charges in Dopamine-Modified TiO_2 and Their Effect on the Formation of Reactive Oxygen Species. *J. Am. Chem. Soc.* **2009**, *131*, 2893−2899.
(47) Xu, J.; Sun, Y.; Huang, J.; Chen, C.; Liu, G.; Jiang, Y.; Zhao, Y.; Jiang, Z. Photokilling Cancer Cells Using Highly Cell-Specific Antibody-TiO_2 Bioconjugates and Electroporation. *Bioelectrochemistry* **2007**, *71*, 217−222.
(48) Thurn, K. T.; Paunesku, T.; Wu, A.; Brown, E. M.; Lai, B.; Vogt, S.; Maser, J.; Aslam, M.; Dravid, D.; Bergan, R.; Woloschak, G. E. Labeling TiO_2 Nanoparticles with Dyes for Optical Fluorescence Microscopy and Determination of TiO_2−DNA Nanoconjugate Stability. *Small* **2009**, *5*, 1318−1325.
(49) Wang, G. L.; Xu, J. J.; Chen, H. Y. Dopamine Sensitized Nanoporous TiO_2 Film on Electrodes: Photoelectrochemical Sensing of NADH Under Visible Irradiation. *Biosens. Bioelectron.* **2009**, *24*, 2494−2498.
(50) Lin, C.-C.; Chu, Y.-M.; Chang, H. C. In Situ Encapsulation of Antibody on TiO_2 Nanowire Immunosensor Via Electro-Polymerization of Polypyrrole Propylic Acid. *Sens. Actuators, B* **2013**, *187*, 533−539.
(51) Luppi, E.; Urdaneta, I.; Calatayud, M. Photoactivity of Molecule-TiO_2 Clusters with Time-Dependent Density-Functional Theory. *J. Phys. Chem. A* **2016**, *120*, 5115−5124.
(52) Vega-Arroyo, M.; LeBreton, P. R.; Zapol, P.; Curtiss, L. A.; Rajh, T. Quantum Chemical Study of TiO_2/Dopamine-DNA Triads. *Chem. Phys.* **2007**, *339*, 164−172.
(53) Vega-Arroyo, M.; Lebreton, P. R.; Rajh, T.; Zapol, P.; Curtiss, L. A. Density Functional Study of the TiO_2-Dopamine Complex. *Chem. Phys. Lett.* **2005**, *406*, 306−311.
(54) Urdaneta, I.; Keller, A.; Atabek, O.; Palma, J. L.; Finkelstein-Shapiro, D.; Tarakeshwar, P.; Mujica, V.; Calatayud, M. Dopamine Adsorption on TiO_2 Anatase Surfaces. *J. Phys. Chem. C* **2014**, *118*, 20688−20693.
(55) Dugandžić, I. M.; Jovanović, D. J.; Mančić, L. T.; Milošević, O. B.; Ahrenkiel, S. P.; Šaponjić, Z. V.; Nedeljković, J. M. Ultrasonic Spray Pyrolysis of Surface Modified TiO_2 Nanoparticles with Dopamine. *Mater. Chem. Phys.* **2013**, *143*, 233−239.
(56) Dovesi, R.; Saunders, V. R.; Roetti, C.; Orlando, R.; ZicovichWilson, C. M.; Pascale, F.; Civalleri, B.; Doll, K.; Harrison, N. M.; Bush, I. J.; et al. *CRYSTAL14 User's Manual*; University of Torino: Torino, Italy, 2014.
(57) Heyd, J.; Scuseria, G. E.; Ernzerhof, M. Hybrid Functionals Based on a Screened Coulomb Potential. *J. Chem. Phys.* **2003**, *118*, 8207−8215.
(58) Grimme, S. Semiempirical GGA-Type Density Functional Constructed with a Long-Range Dispersion Correction. *J. Comput. Chem.* **2006**, *27*, 1787−1799.
(59) Elstner, M.; Porezag, D.; Jungnickel, G.; Elsner, J.; Haugk, M.; Frauenheim, T.; Suhai, S.; Seifert, G. Self-Consistent-Charge Density Functional Tight-Binding Method for Simulations of Complex Materials Properties. *Phys. Rev. B: Condens. Matter Mater. Phys.* **1998**, *58*, 7260−7268.
(60) Elstner, M.; Seifert, G. Density Functional Tight Binding. *Philos. Trans. R. Soc., A* **2014**, *372*, 20120483.
(61) Aradi, B.; Hourahine, B.; Frauenheim, T. DFTB+, A Sparse Matrix-Based Implementation of the DFTB Method. *J. Phys. Chem. A* **2007**, *111*, 5678−5684.
(62) Selli, D.; Fazio, G.; Seifert, G.; Di Valentin, C. Water Multilayers on TiO_2 (101) Anatase Surface: Assessment of a DFTB-Based Method. *J. Chem. Theory Comput.* **2017**, *13*, 3862−3873.
(63) Hu, H.; Lu, Z.; Elstner, M.; Hermans, J.; Yang, W. Simulating Water with the Self-Consistent-Charge Density Functional Tight Binding Method: From Molecular Clusters to the Liquid State. *J. Phys. Chem. A* **2007**, *111*, 5685−5691.
(64) Fazio, G.; Ferrighi, L.; Di Valentin, C. Spherical versus Faceted Anatase TiO_2 Nanoparticles: A Model Study of Structural and Electronic Properties. *J. Phys. Chem. C* **2015**, *119*, 20735−20746.
(65) Labat, F.; Baranek, Ph.; Domain, C.; Minot, C.; Adamo, C. Density Functional Theory Analysis of the Structural and Electronic Properties of TiO_2 Rutile and Anatase Polytypes: Performances of Different Exchange-Correlation Functionals. *J. Chem. Phys.* **2007**, *126*, 154703.
(66) Burdett, J. K.; Hughbanks, T.; Miller, G. J.; Richardson, J. W.; Smith, J. V. Structural-Electronic Relationships in Inorganic Solids: Powder Neutron Diffraction Studies of the Rutile and Anatase Polymorphs of Titanium Dioxide at 15 and 295 K. *J. Am. Chem. Soc.* **1987**, *109*, 3639−3646.
(67) Tang, H.; Lévy, F.; Berger, H.; Schmid, P. E. Urbach Tail of Anatase TiO_2. *Phys. Rev. B: Condens. Matter Mater. Phys.* **1995**, *52*, 7771−7774.
(68) Henkelman, G.; Uberuaga, B. P.; Jonsson, H. A Climbing Image Nudged Elastic Band Method for Finding Saddle Points and Minimum Energy Paths. *J. Chem. Phys.* **2000**, *113*, 9901−9904.
(69) Bahn, S. R.; Jacobsen, K. W. An Object-Oriented Scripting Interface to a Legacy Electronic Structure Code. *Comput. Sci. Eng.* **2002**, *4*, 56−66.

DOI: 10.1021/acs.jpcc.8b04921
J. Phys. Chem. C 2019, 123, 7682−7695